BIOCHEMISTRY
including biophysical chemistry & molecular biology

Article

pubs.acs.org/biochemistry

Ultrafast Fluorescence Decay Profiles Reveal Differential Unstacking of 2-Aminopurine from Neighboring Bases in Single-Stranded DNA-Binding Protein Subsites

Hieu-Ngoc Nguyen, Liang Zhao, Carla W. Gray, Donald M. Gray,* and Tianbing Xia*

Department of Molecular and Cell Biology, Mail Stop FO31, The University of Texas at Dallas, 800 West Campbell Road, Richardson, Texas 75080-3021, United States

Supporting Information

ABSTRACT: Gene 5 protein (g5p) is a dimeric single-stranded DNA-binding protein encoded by Ff strains of *Escherichia coli* bacteriophages. The 2-fold rotationally symmetric binding sites of a g5p dimer each bind to four nucleotides, and the dimers bind with high cooperativity to saturate antiparallel single-stranded DNA (ssDNA) strands. Ultrafast time-resolved fluorescence spectroscopies were used to investigate the conformational heterogeneity and dynamics of fluorescent 2-aminopurine (2AP) labels sequestered by bound g5p. The 2AP labels were positioned within the non-complementary antiparallel tail sequences of $d(AC)_8$ or $d(AC)_9$ of hairpin constructs so that each fluorescent label could probe a different subsite location within the DNA-binding site of g5p. Circular dichroism and isothermal calorimetric titrations yielded binding stoichiometries of approximately six dimers per oligomer hairpin when tails were of these lengths. Mobility shift assays demonstrated the formation of a single type of g5p-saturated complex. Femtosecond time-resolved fluorescence spectroscopy showed that the 2AP in the free (non-protein-bound) DNAs had similar heterogeneous distributions of conformations. However, there were significant changes, dominated by a large increase in the population of unstacked bases from ~22 to 59−68%, depending on their subsite locations, when the oligomers were saturated with g5p. Anisotropy data indicated that 2AP in the bound state was less flexible than in the free oligomer. A control oligomer was labeled with 2AP in the loop of the hairpin and showed no significant change in its base stacking upon g5p binding. A proposed model summarizes the data.

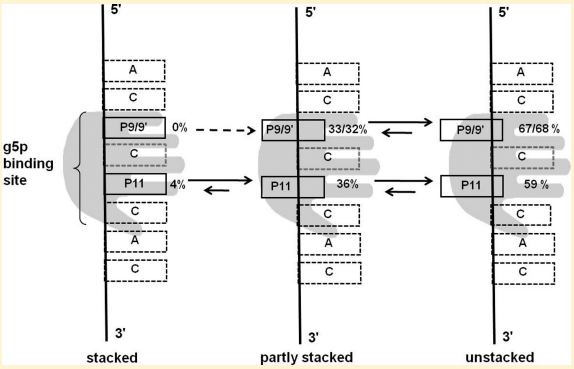

Many vital processes in the cell involve the association of protein with DNA. These interactions can be conformationally dynamic with complex binding mechanisms. For example, the dynamic nature of nucleotides in DNA duplexes is important for recognition of transiently unpaired sequences and subsequent catalysis by some methyltransferases and restriction endonucleases involved in DNA metabolism.[1] Some single-stranded DNA-binding proteins (SSBs), such as eukaryotic RPA, recognize single-stranded DNA (ssDNA) sites to aid in the binding of proteins involved in repair and recombination.[2,3] DNA conformational dynamics may also play an important role in the preferential binding of SSBs to ssDNA sequences that are rich in pyrimidines.[2,4,5] Binding of SSBs alters DNA nucleotide stacking, and the local environment of nucleotides within SSB binding sites differs from that of the free (non-protein-bound) DNA sequences.[5−8] Thus, knowledge of the conformational landscape of nucleotides within SSB binding sites could provide a rich source of information regarding the preferential binding and functioning of SSBs and help to define fundamental differences and similarities among various SSBs.

Ultrafast time-resolved fluorescence spectroscopy has become a highly informative technique for studying the dynamics of binding of proteins and small molecules to RNAs and DNAs, as well as for studying solvation dynamics and photoproduct repair by photolyases.[9−16] In investigations of nucleic acid structure and protein binding, the fluorescent 2-aminopurine (2AP) analogue of adenine has been widely used as a site-specific probe because of its sensitivity to base stacking and its well-characterized decay dynamics.[9−12,14,15,17,18] In this work, we have applied ultrafast fluorescence measurements to explore the conformational heterogeneity of 2AP bound to two different subsite loci of the DNA-binding site of a model SSB, the Ff g5p, as well as to symmetry-related protein binding sites of the g5p dimer.

The g5p is a stable dimer consisting of two identical OB-fold motifs[19,20] that are homologous to those of other SSBs, including the eukaryotic RPA.[21] The g5p dimer exhibits C_2 rotational symmetry,[20] so that it binds to two antiparallel ssDNA strands. It has numerous functions in the life cycle of Ff

Received: April 28, 2011
Revised: September 13, 2011
Published: September 14, 2011

phage, one of which is to saturate nascent circular viral ssDNA genomes, forming a left-handed g5p–DNA complex that is a precursor to the mature phage particle.[22,23] The circular ssDNA is folded back on itself with antiparallel segments bound in the rotationally symmetric binding sites of adjacent, cooperatively bound g5p dimers. The g5p sequesters four nucleotides per monomeric protein binding site in its primary binding mode.[24] The g5p, as well as other SSBs like RPA and *Escherichia coli* SSB, binds with higher affinity to pyrimidine-rich sequences than to purine-rich sequences, in part because of a lower enthalpic cost of unstacking pyrimidine-rich sequences.[2,4,25] However, at least in the case of g5p, ssDNA sequences are not totally unstacked upon g5p binding. While poly[d(A)] and sequences that are rich in d(AA) neighbors are hyperchromic upon being bound by g5p, other sequences, including poly[d(C)], poly[d(T)], poly[d(C-T)], and poly[d(A-C)], show absorbances at 260 nm that are decreased by 8–15% upon g5p binding, indicating that base–base interactions probably occur in g5p-saturated complexes.[4,26]

The conformational heterogeneity of nucleotides bound in individual subsite loci of the g5p binding site, in terms of the populations of nucleotides that are totally and partially unstacked, is unknown. A characterization of this heterogeneity would provide new insight into the binding preferences of this protein and serve as a model for studies involving other SSBs.

An advantage of working with Ff g5p is that it binds with an exceptionally high cooperativity factor (ω) of 500–5000.[27] It should thus be possible to position a 2AP fluorescent label within a defined subsite location in the midst of an array of proteins that are otherwise unperturbed by the label. We designed a DNA oligomer whose central GAAA tetraloop sequence is predisposed to form a stable stem–loop hairpin,[28,29] bringing the two single-stranded ends of the oligomer into an antiparallel alignment favoring simultaneous binding of g5p dimers to the strands. 2AP labels were introduced into four 44-nucleotide oligomer hairpins that have antiparallel tails of 16 alternating A and C bases. These were HPAP-9, HPAP-9′, HPAP-11, and HPAP-loop, illustrated in Figure 1A. If g5p forms equivalently saturated complexes with oligomers HPAP-9 and HPAP-11, which have 2AP labels at the 9th and 11th positions from the 5′ end, respectively, the labels will reside in different subsite positions within a g5p binding site. The 2AP substitution in the 33rd position of the sequence, in the oligomer named HPAP-9′, should be perturbed in a manner similar to that of the 2AP in the 9th position, if the rotationally symmetric monomers of a g5p dimer are aligned as shown in Figure 1A. The HPAP-loop oligomer contains a 2AP label in the loop region of the presumed hairpin fold. This oligomer was included as a control, because its 2AP label is in a portion of the sequence that should not be a preferred binding site of g5p. Oligomer hairpins that were 48 and 36 nucleotides in length, shown in Figure 1B, were used to study the effect of differing tail lengths on the binding stoichiometry. Complexes formed between g5p and these oligomers were characterized by EMSA, CD, and ITC titrations. Finally, the g5p titration of a simple repeating sequence, $d(AACC)_{12}$ (not shown in Figure 1), provided a benchmark for values of the binding affinities and stoichiometries determined from ITC titrations of the hairpin constructs. Subsequent steady-state and time-resolved fluorescence measurements demonstrated for the first time the extent of nucleotide unstacking during g5p binding and allowed an assessment of the heterogeneity of nucleotide populations bound to different subsites of g5p. Anisotropy

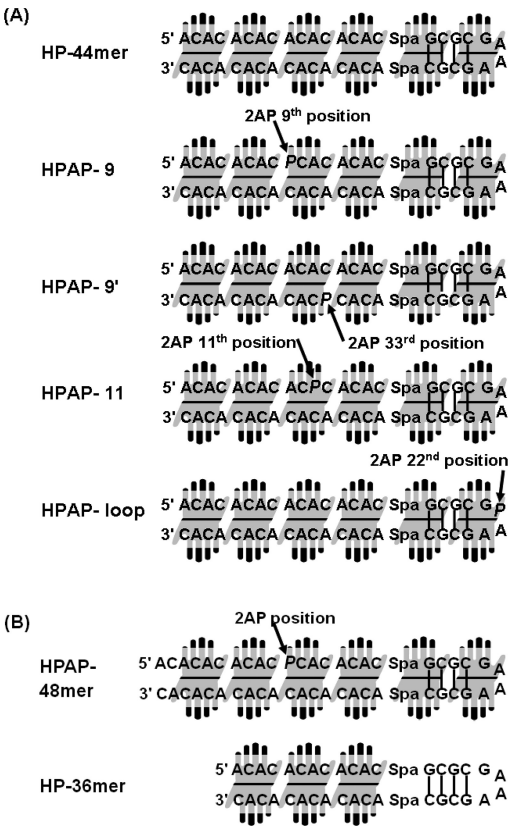

Figure 1. (A) Schematic of DNA 44-nucleotide oligomers designed to have a GAAA tetraloop and a hairpin stem of four G-C base pairs at one end. The hairpin stem is separated from antiparallel tails of 16 alternating A and C bases by triethylene glycol spacers. The oligomer without a fluorescent label is designated as HP-44mer. The positions of fluorescent 2-aminopurine (2AP) labels, denoted as P, are shown in the oligomers named HPAP-9, HPAP-9′, HPAP-11, and HPAP-loop. A possible distribution of six g5p dimers (illustrated as hands) in a saturated g5p–hairpin complex is shown. Regardless of the exact positions of the g5p dimers, the 2AP substitutions at the 9th and 11th nucleotide positions should be in different subsite locations of a g5p monomer within equivalently saturated complexes. The 2AP substitution in the 33rd position of the sequence, in the oligomer named HPAP-9′, should be bound in a subsite of a g5p monomer identical to the subsite location of the 2AP in the 9th position, if the rotationally symmetric monomers of a g5p dimer are aligned as shown. The 2AP substitution in the loop (22nd nucleotide) at the end of the complex should be less perturbed by g5p binding. (B) Schematics of DNA oligomer hairpins with longer and shorter tails. The HPAP-48mer has a 2AP label that, depending on the arrangement of g5p dimers, could be in the same g5p subsite location as the label shown above in HPAP-9. There was no label in the HP-36mer oligomer, which was used to test whether clusters of g5p dimers would bind to the tails of only 12 alternating AC bases.

experiments indicated that there was minimal local motion of the g5p-bound 2AP.

EXPERIMENTAL PROCEDURES

Gene 5 Protein. Fd g5p was isolated by procedures described in previous publications[4,30] with the addition of final purification on a Sephadex G-75 size exclusion column. The protein was concentrated using Millipore (Billerica, MA) Ultra concentrators, with a 10 kDa molecular mass cutoff, and dialyzed against a binding buffer (TN buffer) that consisted of 5 mM Tris-HCl (pH 7.2) and 40 mM NaCl, which was used throughout this

work. The protein was >99% pure as determined by quantitation of bands on SDS–polyacrylamide gels [18% (w/v) resolving and 13% (w/v) stacking] with heated Coomassie staining.[31] The final g5p concentration was 56–89 μM per monomer, determined from absorption measurements using an extinction coefficient of 7074 M^{-1} cm^{-1} (per monomer) at 276 nm.[32] A 276 nm/250 nm ratio of 3.9 indicated the negligible presence of DNA in the purified g5p. An additional sample of purified g5p was kindly provided by T. C. Terwilliger (Los Alamos National Laboratory, Los Alamos, NM).

DNA Oligomers. The unlabeled DNA oligomer designed to be a hairpin, denoted as HP-44mer (Figure 1), had a sequence of 5′-d[$(AC)_8$-spacer-GCGCGAAAGCGC-spacer-$(AC)_8$]-3′, in which the spacers were triethylene glycol $(CH_2)_2O(CH_2)_2O(CH_2)_2$. The fluorescent analogues, HPAP-9, HPAP-9′, HPAP-11, and HPAP-loop, were identical in sequence except that 2-aminopurine (2AP) was substituted for adenosines at positions 9, 33, 11, and 22, respectively. An additional fluorescent analogue, HPAP-48mer, had $d(AC)_9$ tails with a 2AP substitution at the 11th position from the 5′ end, and a nonfluorescent analogue, HP-36mer, had shorter $d(AC)_6$ tails. These oligomers were synthesized by Midland Certified Reagent Co. (Midland, TX), purified via HPLC, and provided as lyophilized ammonium salts. The repeating $d(AACC)_{12}$ oligomer, which did not have a hairpin-forming central sequence, was synthesized by Oligos Etc. (Wilsonville, OR). Each oligomer was dissolved in TN buffer. DNAs were further dialyzed into the same TN buffer for the ITC titrations and for all but two of the samples prepared for ultrafast fluororescence decay and anisotropy measurements (those two being one each of the repeat decay measurements of the HPAP-11 and HPAP-loop complexes). Stock oligomer concentrations (92–143 μM strand concentration) were determined from absorbance measurements using extinction coefficients (per strand) at 260 nm of 3.48×10^5, 4.24×10^5, and 4.62×10^5 M^{-1} cm^{-1} for the 36mer, 44mer, and 48mer hairpin constructs, respectively. The extinction coefficient per strand used for $d(AACC)_{12}$ was 4.55×10^5 M^{-1} cm^{-1}. Extinction coefficients were estimated by a nearest-neighbor calculation[33] with values corrected for nucleotide extinction coefficients determined by Cavaluzzi and Borer.[34] The substitution of 2AP for A could decrease the extinction coefficients of the labeled DNAs by an estimated 2–3%.

Melting Profiles. UV optical melting experiments with the DNA oligomers were conducted in TN buffer using a Shimadzu (Columbia, MD) model 2401PC UV–VIS spectrophotometer. The absorbance at 280 nm was monitored as the temperature was increased from 0, 20, or 25 to 95 °C at a rate of 0.5 °C/min. The percent hyperchromicity at each temperature, T, was calculated with the formula $\%H(T) = 100[\text{absorbance}(T) - \text{absorbance(lowest temperature)}]/[\text{absorbance(lowest temperature)}]$. A Savitzky–Golay 13-point quintic–sexic first-derivative function[35] was applied to find the inflection point, which was used to estimate the melting temperature.

Electrophoretic Mobility Shift Assays (EMSAs). Each DNA construct was radioactively labeled with [γ-^{32}P]ATP using T4 polynucleotide kinase (New England BioLabs, Ipswich, MA). The labeled samples were purified using ProbeQuant G-50 Micro Columns consisting of Sephadex G-50 DNA grade F (GE Healthcare, Piscataway, NJ). Increasing amounts of a known concentration of g5p (18–26 μM dimer concentration) were titrated into samples containing constant concentrations of labeled and unlabeled oligomer (0.01–0.02 and 1.0–1.25 μM final strand concentrations, respectively) in TN buffer. Mixtures were allowed to incubate at room temperature for 30 min, and the samples were electrophoresed on a 2.5% (w/v) low-melting agarose gel at 100 V in TAE running buffer (pH 8.4). The gel was fixed in 50% (v/v) methanol and 10% (v/v) acetic acid and dried for 2 h using a Bio-Rad (Hercules, CA) model 583 gel dryer. The gel was exposed to a Molecular Dynamics phosphor screen and scanned with an Amersham Biosciences Storm 840 scanner (GE Healthcare).

Circular Dichroism (CD) Measurements. DNA samples at 1.0–2.5 μM (strand concentration) were titrated with aliquots of g5p at 26–55 μM (dimer concentration) in TN buffer at 20 °C. After the addition of each aliquot, the mixture was allowed to stand for 5 min at 20 °C before the next addition. CD spectra were recorded over the range from 320 to 190 nm in a 1 cm path length cuvette using a Jasco (Easton, MD) model J715 spectropolarimeter. Spectra were recorded as the average of three accumulations with spectral band widths of 1 nm. Spectra were smoothed at 0.1 nm intervals by a 25-point Savitzky–Golay function provided by Jasco, exported at 1 nm intervals from the Jasco Spectra Manager program, further smoothed by iterations of a Savitzky–Golay 13-point quadratic–cubic function,[35] and finally plotted at 1 nm intervals as molar CD ($\varepsilon_L - \varepsilon_R$), in units of M^{-1} cm^{-1} per mole of nucleotide.

Isothermal Calorimetry Measurements. ITC measurements were performed in TN buffer at 20 °C using a Microcal iTC_{200} microcalorimeter (GE Healthcare). Each titration experiment consisted of 14–20 injections, 2 μL each, of 70–220 μM g5p dimer into 1.0–2.2 μM DNA strand. The initial delay, reference power, and stirring speed were 60–180 s, 5–10 μcal/s, and 1000 rpm, respectively. Injections with a duration time of 4 s were separated by 120 s time intervals. ITC profiles were analyzed using the "One Set of Sites" model in Origin 7 (OriginLab, Northampton, MA). Symmetry-corrected apparent binding affinities per g5p dimer, $K\omega_{app}$, were obtained as described in previous work.[4,30] Correction for the rotational symmetry of g5p required that the binding affinities per g5p dimer from analysis of the ITC profiles be divided by 2. Correspondingly, symmetry-corrected values of $\Delta G°(20\ °C)$ and $\Delta S°$ were obtained by adding values of $RT\ \ln(2) = 403$ cal/mol and $-R\ \ln(2) = -1.38$ cal mol^{-1} K^{-1}, respectively, to the parameters derived from the ITC measurements.[36] Finally, the $K\omega_{app}$ values are derived as if each g5p dimer had the same cooperative interaction, but there are only $N_D - 1$ cooperative interactions for N_D dimers bound to a short oligomer. Thus, our derived $K\omega_{app}$ values are an underestimate of the $K\omega_{pol}$ for a dimer in the midst of a polymeric protein–DNA complex. For example, if the number of dimers bound to a DNA hairpin oligomer is 6, $K\omega_{pol} = K\omega_{app}\omega^{1/6.4}$.[4] If ω is close to the maximum of 5000,[27] $K\omega_{pol}$ would be ~4 times larger than our derived $K\omega_{app}$.

Steady-State Fluorescence Measurements. A Shimadzu RF-5301PC spectrofluorometer was used for steady-state fluorescence measurements. For titration experiments, aliquots of 5.6–10.4 μM concentrated DNA oligomer strand were added to a fixed amount of 0.5 μM g5p dimer or to TN buffer without g5p. The g5p samples were first incubated at 20 °C in TN buffer [5 mM Tris-HCl (pH 7.2) and 40 mM NaCl] for 30 min to allow for equilibration at the binding temperature. Subsequent data were collected after the addition of DNA to 0.5 μM g5p or TN buffer, and equilibration for an additional 2 min at 20 °C was allowed after each addition. Samples of g5p were diluted ≤2% at the end of the titrations. The excitation wavelength was 325 nm, and fluorescence emission was

monitored at 375 nm. The excitation and emission slit widths were set at 5 nm with an instrument response time of 2 s at a low-sensitivity setting. Emission data for samples without buffer were offset to an initial fluorescence value of zero and plotted in arbitrary fluorescence units as a function of the DNA strand concentration.

Ultrafast Time-Resolved Fluorescence Measurements at the Magic Angle. The g5p−DNA complexes were formed at an N_D/S ([g5p dimers]/[DNA strand]) molar ratio of 4.8−5.8 via addition of g5p to 200 μL of oligomer strand at concentrations of ∼85−108 μM. Because there was one 2AP fluorophore per strand, this was also the concentration of the fluorophore. After the addition of protein, which caused dilution of the DNA, the complexes were concentrated in TN buffer at 4 °C to ∼60−95 μM strand using Millipore Amicon Ultracel centrifugal concentrators, with a 10 kDa molecular mass cutoff. CD spectra of the complexes recorded before and after the ultrafast fluorescence experiments confirmed that the DNAs were essentially saturated and that little or no dissociation occurred during the acquisition of the data.

The time-resolved fluorescence experiments were conducted at 22 °C with a previously described instrumental setup.[10,37−39] Briefly, femtosecond pulses (∼120 fs, 800 nm, ∼2.3 mJ) are generated from a Ti:sapphire laser system (Spectra Physics, Irvine, CA). The pulse is used to pump the OPA. The signal output from the OPA is quadrupled to generate the excitation pump pulse at 322 nm. The remainder of the fundamental 800 nm is used as the probe pulse. The 380 nm emission from the sample cell is collected by a pair of parabolic focus mirrors and mixed with the probe pulse in a BBO crystal. The upconverted signal at 257 nm (upconverted from 380 nm) is detected by a photomultiplier after passing through a double-grating monochromator. The pump beam polarization is set at the magic angle (54.7°) with respect to the fluorescence polarization set by the BBO crystal to prevent complications from orientational motions.

In principle, the full femtosecond time-resolved emission spectrum contains information with regard to solvation dynamics[40,41] and DNA dynamics.[42] However, our fluorescence upconversion experiments were performed by monitoring the quenching dynamics of 2AP at a single wavelength (380 nm), close to the emission peak. As shown in Figure S1 of the Supporting Information, the ultrafast hydration dynamic did not produce any abrupt feature within the 0−10 ps time scale transient (neither rise nor decay) at this wavelength for samples in our experiments. Hydration processes would be expected to result in fast transients at longer or shorter wavelengths that were avoided. Therefore, any ultrafast dynamics observed at 380 nm could be attributed to direct charge transfer reactions with a straightforward interpretation of the dynamic information.

Data Analysis of Ultrafast Fluorescence Decay Dynamics. The fluorescent decay profile can be represented by a sum of multiple-exponential functions convoluted by a Gaussian instrument response function as previously described.[10,39] Scientist (Micromath, St. Louis, MO) was used to analyze the ultrafast dynamics data. The minimum number of exponential functions needed to fit a fluorescence decay profile was determined by applying the *F*-test to successive sets of residuals.[10]

The parameter for the slowest component was fixed at the average value (11.3 ns) of the observed lifetimes for free 2AP base, 9-methyl-2AP, and 2AP-riboside (range from 10.4 to 11.8 ns).[43] This is because the time window of the femtosecond experiments (up to 400 ps) is too short to uniquely determine this slowest decay component. The specific choice of the fixed values for this component on the order of 10−11 ns does not affect the fitting of the faster components, but our testing indicated that the fitting may not converge if it is not fixed.[37] Components that are on the order of hundreds of picoseconds can still be determined with data collected over the time window. Uncertainty in the fitted parameters is typically 5%.

Femtosecond Time-Resolved Anisotropy and Data Analysis. Time-resolved anisotropy, $r(t)$, is defined by eq 1:[44]

$$r(t) = \frac{I_{\parallel}(t) - I_{\perp}(t)}{I_{\parallel}(t) + 2I_{\perp}(t)} \quad (1)$$

where $I_{\parallel}(t)$ and $I_{\perp}(t)$ are calibrated time-dependent fluorescence intensities with emission polarization parallel and perpendicular to that of the excitation, respectively, collected separately.[10,12,37] The signal intensity of 2AP at −10 ps (in the negative time regime) was used for background correction. To account for possible excitation power fluctuation between the separate measurements of parallel and perpendicular polarization intensities, we measured the fluorescence intensities for a solution of free 2AP base at a long delay time (e.g., 400 ps), following acquisition of each transient for the samples. At a time delay of 400 ps, the anisotropy of free 2AP base should have completely decayed to zero, and identical intensities of 2AP fluorescence should be observed for the parallel and perpendicular polarizations. Differences in the intensities were used to calibrate the two polarization transients of the samples. Femtosecond time-resolved anisotropy, $r(t)$, constructed using eq 1, was then fitted with a multiple-exponential function. Two decay terms were sufficient to fit the decay profiles in this work. Setting initial values of the slower decay term at values of >4 ns did not significantly affect the amplitude of the faster decay term, which represented segmental or internal motions of the probe that reflected its intrinsic mobility in different contexts[12,37] (see Figure S2 of the Supporting Information).

RESULTS

Formation of Oligomer Hairpins and a Single Type of Complex. The oligomers sketched in Figure 1 contained a central GCGCGAAAGCGC sequence with four G-C base pairs and a GAAA tetraloop favorable for hairpin formation.[28,29] Derivatives of absorbance melting profiles of six of these gave melting temperatures of ∼80 °C in TN buffer for the free DNA oligomers, several of which were tested over a 6-fold concentration range (see Figure S3 of the Supporting Information). This T_m was slightly higher than the T_m of 76.5 °C for a GCGAAAGC hairpin that has a stem of only two G-C base pairs [in 0.1 M NaCl and 50 mM sodium cacodylate (pH 7.0)].[28,29] In addition, gel electrophoresis of multiple samples of radioactively labeled HP displayed only one band over a 500-fold concentration range from 0.14 to 74 μM per strand (data not shown). We concluded that our oligomers most likely existed as monomeric hairpins under the conditions in which g5p was added to form complexes.

An example EMSA titration of labeled HP-44mer oligomer with g5p, performed as described in Experimental Procedures, is shown in Figure 2A. Comparable results were obtained in EMSA experiments with the other hairpin oligomers, as shown in Figure S4 of Supporting Information. The labeled DNA was shifted to form only one major low-mobility band as g5p was added to give increasing N_D/S molar ratios. The absence of

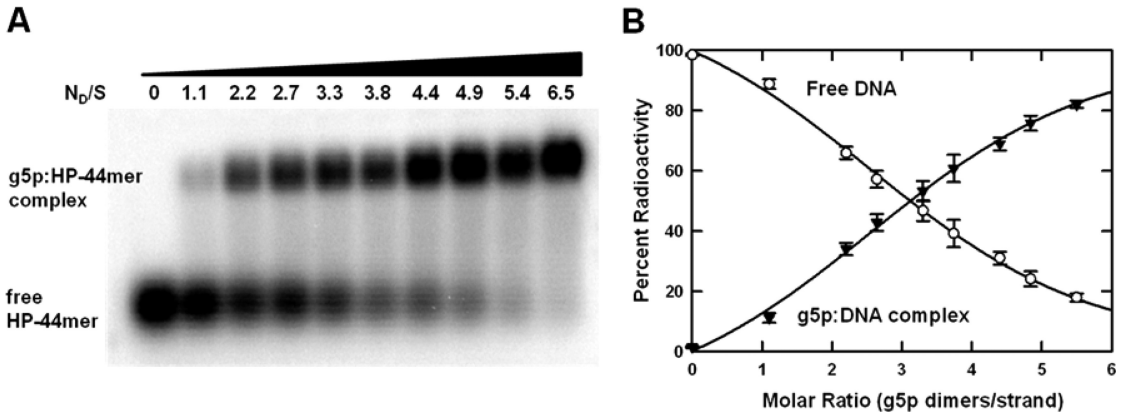

Figure 2. (A) EMSA results from the titration of the ^{32}P-labeled DNA HP-44mer oligomer with g5p. The N_D/S ([g5p dimers]/[DNA strand]) molar ratio is indicated at the top of each lane. Samples were run on 2.5% native agarose gels. The band of higher mobility is that of the free DNA oligomer, while the band of lower mobility is the result of formation of g5p–DNA complexes. There were no significant bands of intermediate mobility. The buffer was TN buffer [5 mM Tris-HCl (pH 7.2) and 40 mM NaCl] for the mixtures subjected to EMSA and for the data presented in Figures 3–7. (B) Averaged data from EMSA binding profiles for four samples of the 44-nucleotide oligomers, two each of HP-44mer and HPAP-9. As the N_D/S molar ratio increases, the percentage of radioactivity in the free DNA band decreases (○) and the percentage of radioactivity in the g5p–DNA complex band increases (▼). Saturation of the DNA occurred with approximately six dimers of g5p. Error bars show one standard deviation.

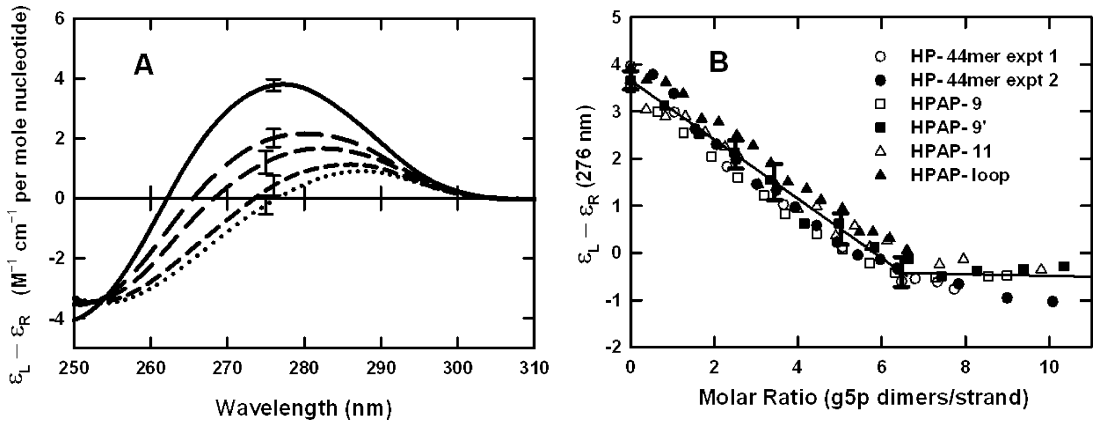

Figure 3. (A) CD spectra of DNA oligomers titrated with g5p. Spectra shown are from an example titration of HPAP-11 with g5p. N_D/S molar ratios of the spectra were 0 [i.e., free DNA (—)], 2.6 (— — —), 3.5 (– – –), 5.1 (---), and 6.4 (···). Additional spectra were recorded at other N_D/S molar ratios but were omitted for the sake of clarity. CD spectral changes for all five 44-nucleotide oligomers were essentially the same (error bars show one standard deviation from five or six sets of spectra for panels A and B). (B) CD values at 276 nm as a function of N_D/S molar ratio from titrations of all five 44-nucleotide oligomers with g5p.

discrete bands of intermediate mobility showed that g5p binds to the oligomer hairpins to saturate them in an approximately all-or-none manner, consistent with the high binding cooperativity of g5p.[27] There was no evidence of the existence of more than one discrete type of complex. Saturation of the 44mers occurred at an N_D/S ([g5p dimers]/[DNA strand]) molar ratio of ~6 (Figure 2B). If it is assumed that an average of 5.5–6.0 dimers bind in a cluster per strand, the average $K\omega_{app}$ per dimer can be estimated as $1/(2L)$, where L is the free dimer concentration at 50% saturation and the factor of 2 takes into account the 2-fold symmetry of g5p dimer binding.[4,30] From the EMSA titrations of the 44mers plotted in Figure 2B, $K\omega_{app}$ was estimated to be $1.0–3.2 \times 10^6$ M^{-1}, which was in reasonable agreement with more accurate results from ITC titrations, discussed below.

The g5p–Oligomer Complexes All Have Similar CD Characteristics. The near-UV CD spectra of five of the 44mer DNA oligomers at 20 °C were all similarly perturbed in titrations with g5p in TN buffer and are represented by the example titration of HPAP-11 in Figure 3A. In the near-UV region of 250–300 nm, the CD spectrum of g5p itself is negligible on the scale shown.[7] The CD spectra of the free DNA oligomers and the effects of g5p binding were the same, within the error of measurement, for all of the hairpin DNAs illustrated in Figure 1, including the 36- and 48mer DNAs (not shown). Although there is no simple interpretation of these spectral changes, they are reflective of alterations in DNA base–base interactions and nucleotide conformations, with no significant direct optical contributions due to the protein or protein–DNA interactions.[5,7,24] There was an approximate isodichroic point at 252–254 nm, indicative of a two-state transition.

Figure 3B is a plot of CD values at 276 nm as a function of the N_D/S molar ratio obtained from multiple titrations. Consistent with the EMSA results, there was a breakpoint in the CD titrations close to an N_D/S ratio of ~6, indicating that approximately six g5p dimers are needed to saturate a 44mer oligomer strand. We assume that binding of g5p was in its

dx.doi.org/10.1021/bi2006543 | Biochemistry 2011, 50, 8989–9001

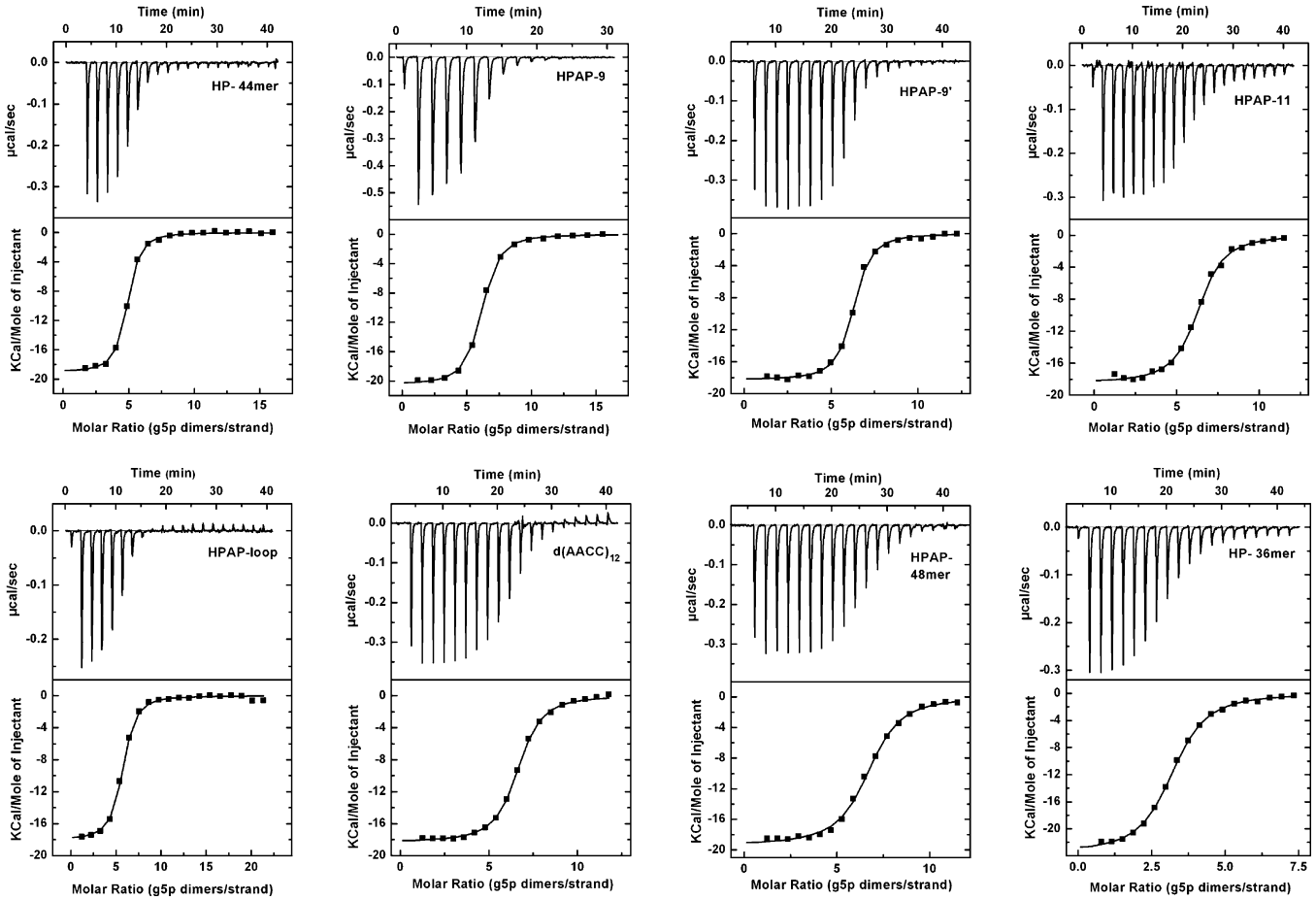

Figure 4. Representative isothermal calorimetry titrations at 20 °C of all seven oligomer constructs shown in Figure 1, and a nonhairpin 48-nucleotide oligomer, $d(AACC)_{12}$. A constant amount of g5p was added at every titration point except for the initial injection. Top panels show the raw titration data. Bottom panels show the integrated heat response as a function of the g5p dimer/DNA strand (N_D/S) molar ratio. Data at high molar ratios were taken as baseline values. The One Set of Sites model (Origin 7) was used to fit the data (solid lines in the bottom panels), and results are listed in Table 1 for titrations of all oligomers.

primary n = 4 binding mode (n being the number of nucleotides bound per g5p monomer binding site).[24,26] Because only four g5p dimers can be accommodated on the single-stranded 16-nucleotide tails of the DNA 44mer hairpins, up to two more protein dimers apparently associate with the stem−loop region of the hairpin, suggesting that the protein binds in a cluster that is stabilized by strong cooperative binding.

ITC Profiles Are Fitted by a Single Type of Sites Model. Representative ITC profiles obtained by titrating each of the five hairpin sequences of Figure 1A with g5p are shown in Figure 4. The titrations were conducted at 20 °C in TN buffer. Thermodynamic parameters listed in Table 1 were derived using Origin 7 and a "One Set of Sites" model with the assumption that protein dimers are equivalent in their binding to multiple lattice sites on a given DNA strand. The binding profiles were well fitted and consistent with this assumption, giving averaged parameters for all the g5p dimers within a cluster on a given hairpin strand. From multiple ITC experiments with DNA hairpins of 44 nucleotides, the average $K\omega_{app}$ was $(4.08 \pm 1.34) \times 10^6$ M^{-1} and the number, N_D, of g5p dimers bound per DNA strand was 5.6 ± 0.4 (top section of Table 1). The binding of the g5p to the hairpin oligomers is characterized by negative values of both enthalpy and entropy and is therefore enthalpically driven, as is the case for binding of the *E. coli* SSB and the human replication protein A to ssDNA.[45−47]

The number of g5p dimers that bind to the 44mer hairpin constructs was greater than that needed for saturation of just the single-stranded tails and implied that approximately two additional dimers were associated with the hairpin loop and spacer, perhaps weakly. ITC titrations of additional oligomers were performed to assess this possibility (Figure 4 and bottom section of Table 1). First, ITC titration of a control ssDNA $d(AACC)_{12}$ oligomer resulted in the expected number of 12 g5p dimers being associated with two antiparallel strands of the oligomer, or 6 dimers per strand, for binding of the g5p in its n = 4 binding mode. In previous work, CD titration end points gave 6.3 ± 2 dimers bound per strand of this oligomer.[4] Thus, from this control, we were assured that 5−6 dimers bind to our 44mer hairpin constructs in a cluster extending beyond the ssDNA tails.

Second, ITC titrations were performed with 48- and 36mer hairpin oligomers (Figure 1B) having longer and shorter tails of repeating d(AC) sequences of 18 and 12 nucleotides, compared with the 16-nucleotide tails of the 44mer oligomers. The N_D/S value of 6.4 ± 0.1 for the HPAP-48mer was marginally greater than the N_D/S value of 5.6 ± 0.4 for binding to the 44mers. However, the number of dimers that bound per HP-36mer was decidedly fewer, 3.1 ± 0.1, suggesting that the protein bound to

dx.doi.org/10.1021/bi2006543 | *Biochemistry* 2011, 50, 8989−9001

Table 1. Parameters from ITC Titrations at 20 °C of DNA Hairpins with g5p[a]

DNA oligomer	N_D/S (no. of g5p dimers per DNA hairpin or strand)	$K\omega_{app} \times 10^{-6}$ (M^{-1})	$\Delta G°$(20 °C) (kcal/mol of g5p dimer)[b]	$\Delta H°$ (kcal/mol of g5p dimer)	$\Delta S°$ (cal mol^{-1} K^{-1})[b]
HP-44mer	5.0 ± 0.4	4.91 ± 1.33	−9.0 ± 0.2	−19.7 ± 1.5	−36.8 ± 6.5
HPAP-9	5.6	3.21	−8.7	−20.5	−40.3
HPAP-9′	6.0 ± 0.2	5.81 ± 0.39	−9.1 ± 0.1	−18.3 ± 0.1	−31.6
HPAP-11	6.0	2.41	−8.6	−18.4	−33.7
HPAP-loop	5.2 ± 0.9	4.04 ± 1.26	−8.8 ± 0.2	−19.1 ± 1.0	−34.9 ± 3.0
avg ± SD for 44mers	5.6 ± 0.4	4.08 ± 1.34	−8.8 ± 0.2	−19.2 ± 0.9	−35.4 ± 3.3
$d(AACC)_{12}$	6.0	3.50	−8.4	−18.3	−33.9
HPAP-48mer	6.4 ± 0.1	2.00 ± 0.1	−8.0 ± 0.1	−19.7 ± 0.3	−39.8 ± 1.1
HP-36mer	3.1 ± 0.1	1.78 ± 0.1	−8.0 ± 0.1	−23.3 ± 0.2	−52.3 ± 0.7

[a]Values are from fits using a single type of sites model (by Origin). $K\omega_{app}$, $\Delta G°$, and $\Delta S°$ values are symmetry-corrected for binding of the g5p dimer. Averages for N_D/S, $K\omega_{app}$, and $\Delta H°$ were calculated from five and three sets of titration data for HP-44mer and HPAP-loop DNA, respectively, and from two sets of data for HPAP-9′, HPAP-48mer, and HP-36mer DNA. Errors for individual DNA hairpins are standard deviations for HP-44mer and HPAP-loop DNA and the range of measurements for HPAP-9′, HPAP-48mer, and HP-36mer DNAs. Data for HPAP-9, HPAP-11, and $d(AACC)_{12}$ are from single titrations. [b]Calculated as $\Delta G°(20°) = -RT \ln(K\omega_{app})$ and $\Delta S° = -(\Delta G° - \Delta H°)/T$, with propagated errors. Titrations were performed at 20 °C in TN buffer.

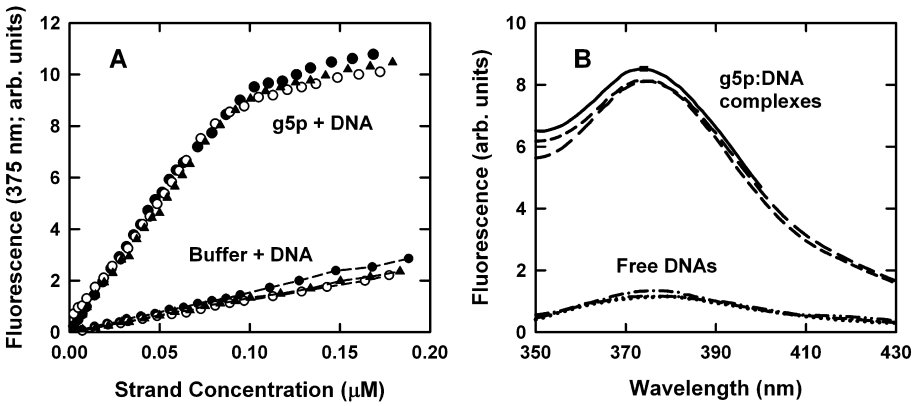

Figure 5. (A) Steady-state fluorescence titrations of g5p or buffer with three DNA oligomers. One set of curves [HPAP-9 (●), HPAP-9′ (○), or HPAP-11 (▲)] was obtained by adding aliquots of concentrated DNA oligomers to a solution of 0.5 μM g5p dimer in TN buffer at 20 °C. Another set of curves (dashed lines with the same symbols) was obtained by adding aliquots of the same DNAs to TN buffer at 20 °C. The 2-aminopurine of the DNA was excited at 325 nm, and its emission at 375 nm was monitored. The change in fluorescence, minus buffer and with an initial offset to zero, is plotted as a function of strand concentration for each titration. (B) Fluorescence spectra of DNAs that were added to g5p to give N_D/S ratios of 5.7−6.2 [HPAP-9 (—), HPAP-9′ (– – –), or HPAP-11 (---)], compared with spectra of the respective free DNAs at the same DNA concentrations [HPAP-9 (—·—), HPAP-9′ (—··—), or HPAP-11 (···)]. The final DNA concentrations were similar (0.084−0.089 μM per strand) for all the spectra.

the ssDNA tails and that, once the tail length was reduced to 12 nucleotides, a g5p cluster of three dimers did not generate sufficiently stable cooperative interactions to cause concomitant binding to the stem−loop region of the hairpin, at least not in a manner that resulted in a detectable exothermic reaction. We conclude that the 44mers allow g5p dimers to bind in stable clusters extending beyond the ssDNA tails and that, within such clusters, fluorescent labels could be positioned to probe specific subsites within a given g5p dimer.

The 2AP in the G5p Binding Site Is Significantly Unstacked. As seen in Figure 5A, the steady-state fluorescence of 2AP-labeled DNA oligomers HPAP-9, HPAP-9′, and HPAP-11 was dramatically increased when the oligomers were titrated into a solution of 0.5 μM g5p dimer, compared with the fluorescence of the oligomers when they were added to TN buffer. Thus, the fluorescence of 2AP was less quenched when bound by g5p, which we interpret to mean that the 2AP was unstacked and interacted less with neighboring cytosines in the bound state than when in a free single strand. The curves for titrations of the different DNA oligomers added to g5p were essentially indistinguishable in the extent of fluorescence increase per strand and were similar in having approximate breakpoints at strand concentrations of 0.087−0.096 μM (N_D/S ratios of 5.2−5.7). Beyond these breakpoints, the slopes of the curves for additions of the DNA to g5p were close to those for the additions of DNA to buffer alone. A very similar result was obtained from the steady-state fluorescence titration of HPAP-48mer, shown in Figure S5 of the Supporting Information.

The fluorescence spectra for the free and complexed HPAP-9, HPAP-9′, and HPAP-11 DNA oligomers at strand concentrations of 0.084−0.089 μM (N_D/S ratios of 5.7−6.2) are shown in Figure 5B. At these strand concentrations, the measured apparent increase in steady-state fluorescence at 375 nm due to binding of g5p was 6−7-fold. Moreover, using the $K\omega_{app}$ determined from ITC measurements, we estimate that the extent of saturation was ≥60% of the strands under

dx.doi.org/10.1021/bi2006543 | Biochemistry 2011, 50, 8989−9001

these conditions, so that the increase in 2AP fluorescence for a fully g5p-saturated solution of DNA oligomers could be as much as 1.5 times higher than measured.

The fluorescence of 2AP in the control HPAP-loop DNA was only weakly perturbed by the binding of g5p (shown in Figure S6 of the Supporting Information), with less than 5% of the increase found for binding of the other 2AP-labeled DNAs. This was consistent with the expectation that a label in the loop region of a DNA hairpin would not be a preferred binding site for g5p (Figure 1).

Ultrafast Time-Resolved Fluorescence Spectroscopy Demonstrates a Shift in Heterogeneous Populations and Reduced Flexibility of 2AP upon g5p Binding. Ultrafast time-resolved decay profiles for the free 44mer DNAs, HPAP-9, HPAP-9′, and HPAP-11, are plotted in the top three panels of Figure 6 (data shown as circles). The profiles for these three DNAs were essentially indistinguishable and were each characterized by three significant exponential decay components from fits performed as previously described.[10] The decay times and amplitudes are listed in the top half of Table 2. A decay profile for a longer DNA, HPAP-48mer, is included in Figure S7 of the Supporting Information, and its decay parameters are included in Table 2. It was not unexpected that profiles would be similar for all four of these free DNAs because the local sequence contexts of 2AP were all the same, with the 2AP being flanked by cytosines. The longest decay time of 11300 ps was chosen as being characteristic of the isolated 2AP base and was fixed in such analyses because the time window of the femtosecond experiments, at up to 400 ps, was too short to independently determine the slowest component, which might be as short as 3000 ps for 2AP in ssDNA.[10,43,48] In any case, the results of fits to the decay profiles for these four DNAs were not very sensitive to the choice of the longest decay component [even with values as short as 3000 ps (not shown)]. The amplitude of the slowest component, which averages to be ~22% from the data in Table 2, may be considered to represent the population of 2AP that is least stacked so that its fluorescence is least quenched by static or dynamic stacking in the single-stranded tails of these DNA hairpins.

At the other extreme of decay times, the amplitude of 2AP showing the fastest decay kinetics at 17−37 ps is attributed to the most stacked and statically quenched conformations.[10,49] The 44mers, HPAP-9, HPAP-9′, and HPAP-11, exhibited an average of 18% of this fastest decay component. Their dominant population of ~60% decayed at intermediate times of 142−188 ps. Components in this range of lifetimes are not necessarily indicative of single 2AP/quencher states that determine the charge transfer times. They could be influenced by motions on this time scale that gate the charge transfer reactions involving 2AP.[49] Indeed, anisotropy decay data shown in Figure 7, with analyses given in Table 3, indicated that there were significant motions taking place at 145−183 ps for these three isolated DNAs. Moreover, as explained in Experimental Procedures, there was no evidence of an effect of hydration dynamics that might complicate an interpretation of the decay profiles as monitored at 380 nm. Therefore, we conclude that the intermediate fluorescent decay times for HPAP-9, HPAP-9′, and HPAP-11 represent a combination of static quenching and the effects of motions that gate charge transfer and quenching. The data for HPAP-48mer show that it was similar to the labeled 44mers in its fluorescence and anisotropy decay profiles (Tables 2 and 3).

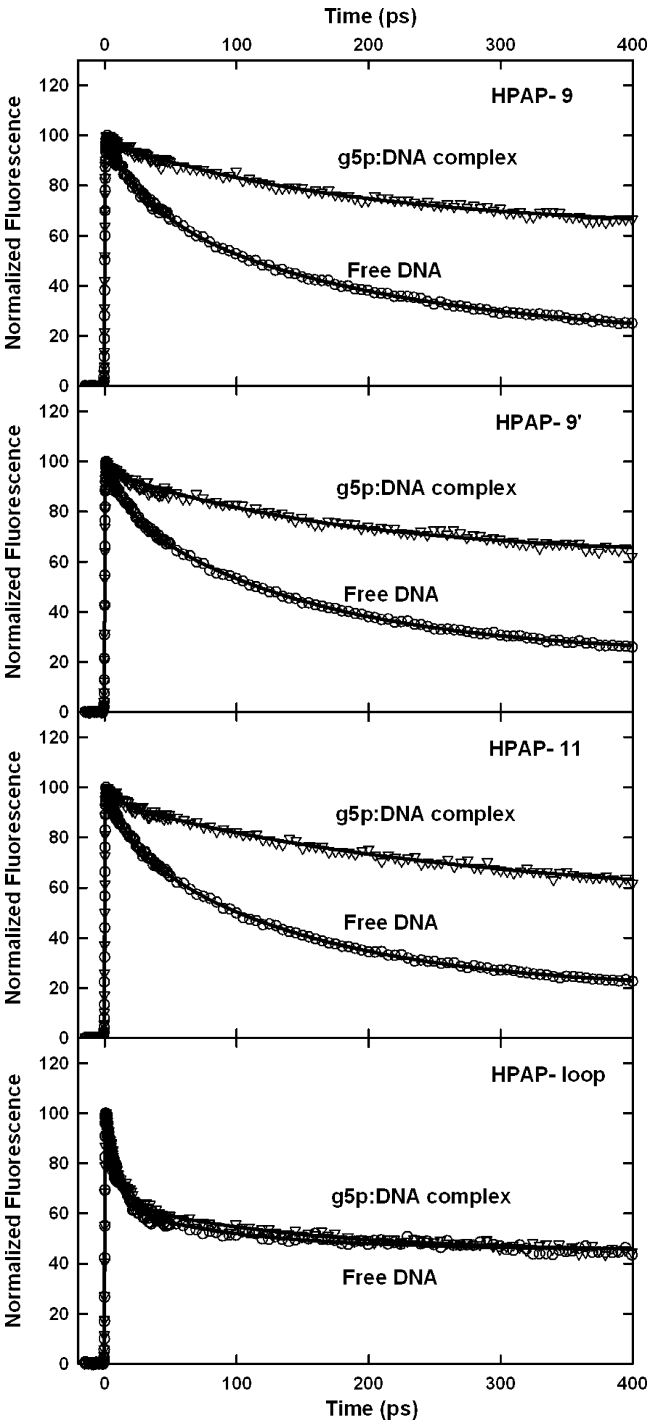

Figure 6. Representative ultrafast fluorescence decay profiles of the 2-aminopurine in HPAP-9, HPAP-9′, HPAP-11, and HPAP-loop DNA oligomers, free and saturated with g5p. The 2-aminopurine was excited at 322 nm, and its emission decay was monitored at 380 nm, normalized to a value of 100 at time zero. Experimental data are shown as circles (free DNA) or triangles (complexes), and the solid lines are fitted curves with two or three exponential terms, the minimum number that was statistically significant as determined by the *F*-test.[10] Decay times and amplitudes are listed in Table 2.

While specific structures that correspond to the fluorescent decay components have not been identified, we envision the multiple decay times to be associated with three generic types of conformation illustrated in simplified form in Figure 8A for the HPAP-9, HPAP-9′, and HPAP-11 44mer DNAs, all of

dx.doi.org/10.1021/bi2006543 | *Biochemistry* 2011, 50, 8989−9001

Table 2. Parameters of Femtosecond Time-Resolved Fluorescence Decays

	DNA hairpin	significant component decay times (ps)[a] (% amplitudes)		
free DNA hairpin[b]	HPAP-9	17−33 (20 ± 5%)	143−188 (57 ± 1%)	11300 (23 ± 3%)
	HPAP-9′	17 (17%)	144 (60%)	11300 (24%)
	HPAP-11	21 (17%)	142 (62%)	11300 (20%)
	HPAP-loop	8 (38%)	84 (16%)	11300 (46%)
	HPAP-48mer	37 (26%)	195 (53%)	11300 (21%)
g5p−DNA complex[c]	HPAP-9		174 (33%)	11300 (67%)
	HPAP-9′		165 (32%)	11300 (68%)
	HPAP-11	7−18 (4 ± 1%)	240−262 (36 ± 2%)	11300 (59 ± 2%)
	HPAP-loop	8−9 (34 ± 2%)	123−135 (20 ± 2%)	11300 (46 ± 1%)
	HPAP-48mer		148 (32%)	11300 (68%)

[a]Decay curves were fit with two or three exponential terms; the decay time of 11300 ps is characteristic of the isolated 2AP base and was fixed.[10,43,48] [b]The longest decay time is likely shorter for free DNAs. See the text. [c]Complexes with the 44mers were all formed at N_D/S ratios of 4.8−5.8 to obtain data for this table and Table 3. Ranges of decay times are shown for duplicate measurements of the HPAP-9 DNA and HPAP-loop complex and for triplicate measurements of the HPAP-11 complex. Amplitudes are averages with errors that are ranges in the case of duplicate measurements and the standard deviation in the case of triplicate measurements. Percentages are rounded to the nearest 1%.

which have 2AP sandwiched between cytosines. This figure summarizes the equilibrium between the states, with the reasonable assumption that a partly stacked population is intermediate between the most-stacked and least-stacked populations. The figure is not intended to imply any coordination of the conformational states of the three positions within a given DNA strand.

The decay of 2AP in the HPAP-loop free DNA, which was labeled within the hairpin loop sequence at the 22nd position and flanked by purines, was quite unlike that of the other free DNAs. In this case, the greatest population of states, 46%, was unstacked, and 38% decayed with the fastest decay time, indicative of static quenching by neighboring bases. Thus, the sequence context of the label influenced its decay profile within the free DNA and confirmed that the heterogeneity of the 2AP population was essentially equivalent in the other three sequence contexts.

Femtosecond decay profiles of the g5p−DNA complexes that were obtained by saturating the DNAs with g5p were markedly different in the percentages of populations having different decay times, compared with those of the free DNAs. [Approximately 98% of the DNA was saturated with protein in the complexes used for fluorescence dynamics and anisotropy (see the discussion in the Supporting Information).] Most notable from the decay profiles of the complexes was the larger percentage of the slowest component, attributed to the unstacked population of 2AP bound to g5p in the (A+C)-rich tails of the hairpins, as shown in Figure 6, Figure S7 of the Supporting Information, and the bottom half of Table 2. When sequestered by g5p, the 2AP probes in HPAP-9 and HPAP-9′ had unstacked populations of 67−68%, while that in HPAP-11 was unstacked to a slightly lesser extent (59%). Populations of the faster decay components were correspondingly decreased relative to those of the free DNAs.

These results were in agreement with the expectation that HPAP-9 and HPAP-9′ would have the 2AP identically sequestered in rotationally symmetric sub-binding site positions of a g5p dimer. Moreover, compared with the unstacked populations in the free DNAs, the increase in the unstacked population in HPAP-9 and HPAP-9′ was 1.2 times greater than the increase in the unstacked population in HPAP-11 [i.e., $(67.5 - 22)/(59 - 22) = 45.5/37 \approx 1.2$]. This difference in the unstacked populations, along with 3−4% differences in the populations of faster components, indicated that there were differences among the binding subsites of g5p that could be detected by ultrafast fluorescence measurements. These points are illustrated in Figure 8B, which shows the differences in the heterogeneity of the 2AP in the 9th and 11th g5p subsite locations when bound by g5p.

Decay parameters for the g5p−HPAP-48mer complex were interesting because they were closer to those of HPAP-9 and HPAP-9′ than to those of HPAP-11, including a 68% fraction of an unstacked population (Table 2). This implied that the cluster of protein dimers may have been associated with the oligomer in approximately the phase shown in Figure 1B, so that the 2AP label of HPAP-48mer was preferentially sequestered in the same protein subsite as when the label was in the shorter HPAP-9 oligomer. Thus, a tentative conclusion is that the position of the protein cluster appeared to be influenced more by the stem−loop end of the hairpin oligomer than by the ends of the ssDNA tails.

In contrast to the free DNAs, there was no evidence from anisotropy decay profiles (see Figure 7 and Figure S7 of the Supporting Information) for significant independent local motion of the 2AP in the HPAP-9, HPAP-9′, HPAP-11, and HPAP-48mer oligomers once the DNAs were in complexes with g5p. The presence of a dominant slow anisotropy decay component (Table 3) undoubtedly represented the tumbling of the entire molecule, because the rotational correlation time of the g5p dimer is 12.9 ns.[50] We conclude from the anisotropy results that the various states of 2AP sequestered within the g5p binding site represented relatively inflexible conformations.

Finally, 2AP in the 22nd position in the HPAP-loop DNA was less perturbed in its decay pattern by g5p binding than were the 2AP labels in the other DNAs (Figure 6 and Table 2), with the retention of three decay times and with no major change in the percentage of unstacked bases, in agreement with the steady-state fluorescence measurements. Anisotropy data showed that the 2AP in the g5p−HPAP-loop complex was also relatively inflexible, but with a slightly larger amplitude of a 54−107 ps component. The differing decay dynamics for 2AP in the HPAP-loop oligomer compared with those of 2AP in the other oligomers, with and without bound g5p, indicated that 2AP was only marginally affected by g5p binding when it was not wholly within a normal g5p binding site.

DISCUSSION

The g5p, as well as other SSBs like *E. coli* SSB and human replication protein A, binds with higher affinity to pyrimidine-rich

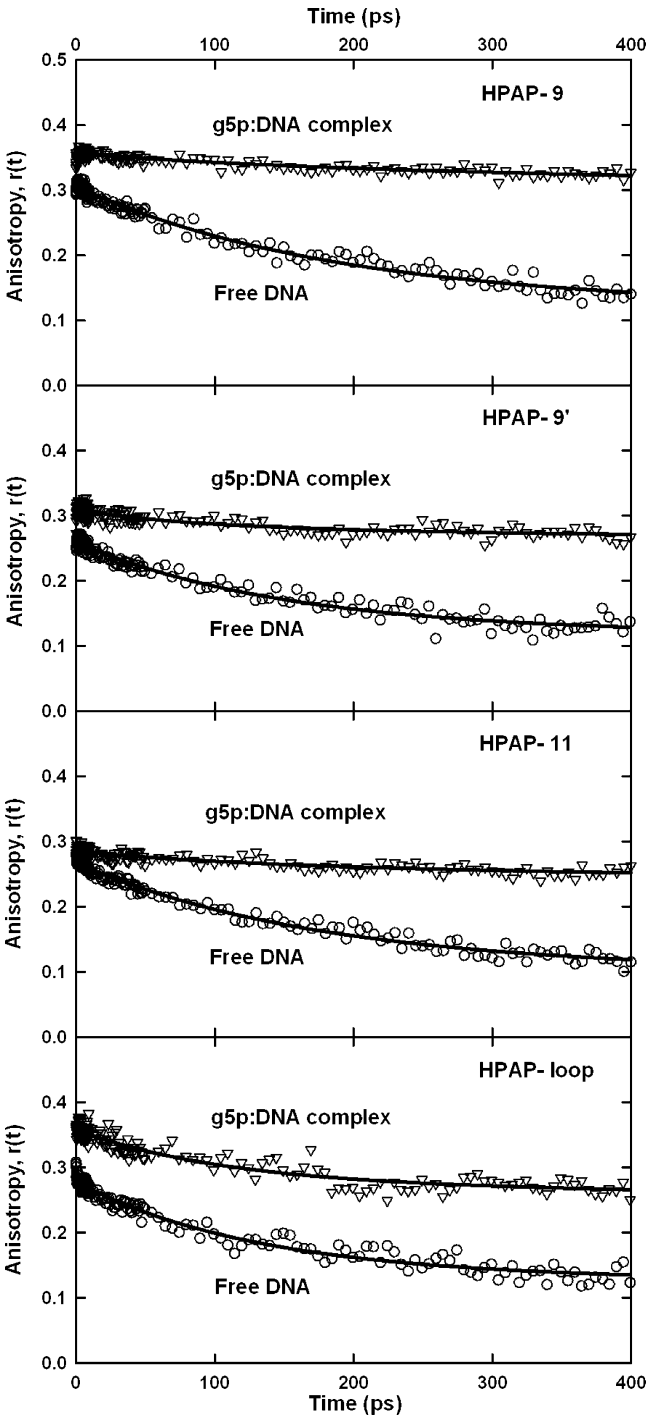

Figure 7. Representative ultrafast anisotropy decay profiles of the 2-aminopurine in HPAP-9, HPAP-9′, HPAP-11, and HPAP-loop DNA oligomers, free and saturated with g5p. Experimental data are shown as circles (free DNA) or triangles (complexes), and the solid lines are fitted curves. At most, two exponential terms were needed to fit the data,[10] yielding the results listed in Table 3.

sequences than to purine-rich sequences, due in part to a preference for binding to pyrimidine-rich sequences driven by the lower enthalpic cost of unstacking such sequences.[2,4,25] In addition, the inherent tendency for nucleotide sequences to stack with a right-handed twist suggests that the nucleotides would have to be at least partly unstacked during g5p binding to allow the formation of g5p−ssDNA complexes having a left-handed helical structure.[20,22] However, at least in the case of g5p, ssDNA sequences are not totally unstacked upon binding of g5p, as indicated by absorbance measurements described in the introductory section to this paper.[4,26] In this work, for the first time, we have been able to quantitate the unstacking of a 2AP fluorescent label within a C-2AP-C sequence context when sequestered within different subsite loci of the DNA-binding site of g5p. The percentage of 2AP bases not stacked with neighboring cytosines was increased from ∼22% in the free DNAs to 59−68% in the g5p-bound DNAs, leaving a remaining population of stacked bases of between 32 and ∼40% (see Table 2 and Figure 8). Moreover, we have been able to explore for the first time the heterogeneous nature of the states of a nucleotide bound by g5p. Differences in the time-resolved fluorescence data for 44mers HPAP-9/9′ and HPAP-11 showed that subsite locations of the bound 2AP detectably affect the pattern of heterogeneity, including the relative proportions of stacked versus unstacked bases, albeit less than might have been expected from the variety of protein−nucleotide interactions that potentially can occur within a given binding site. Finally, results for the longer HPAP-48mer oligomer show that subsite differences in the dynamics of g5p-bound 2AP might be used to investigate the positioning of clusters of g5p dimers on hairpins that differ in tail length and other features.

Although there is no crystallographic structure for a g5p−nucleic acid complex, and the DNA strand orientation in the binding site is not known, NMR data show that there are subsites in which the bases of $d(A)_n$ oligomers interact with specific protein side chains.[51] Leu and Phe side chains have been proposed to stack with, and sequester, one of the bases in the binding site, while Tyr26 may either form a hydrogen bond to the sugar−phosphate backbone or stack with another base.[51] Moreover, protein residues essential in binding ssDNA are located in a flexible β-ribbon that may well contribute to a diversity of interactions needed for nonspecific ssDNA binding.[20,52,53]

On the other hand, 500 MHz ^{1}H NMR experiments with the g5p−$d(A)_{40-60}$ complex[51] showed no heterogeneity in adenine ring H2 and H8 and sugar H1′ resonances in saturated g5p−$d(A)_{40-60}$ complexes, but rather single resonances for each of these protons in the bound state, resonances that differed from those for the free base (over a temperature range of 5−35 °C and from 0 to 200 mM NaCl), suggesting that the bound bases experience similar environments. One possibility is that in the case of g5p binding to the uniform sequence in $d(A)_{40-60}$ the bases are able to move between neighboring subsites on a submillisecond time scale.[51] Our data now show that, when detected on a fast picosecond to nanosecond time scale, the unstacked populations of 2AP in the alternating $d(AC)_8$ sequence and the dominant effects of binding are similar, but not identical, within two different subsites of g5p.

Relatively long anisotropy decay components of >4 ns for 2AP labels in the free DNAs and g5p−DNA complexes are consistent with the rotational correlation times of the whole molecules.[15,50,54] Although the rotational correlation times for the free DNAs are undoubtedly shorter than those for the complexes,[50,54] they should all be >4 ns, and, as explained in Experimental Procedures and shown in Figure S2 of the Supporting Information, values of the longer of two decay times above 4 ns did not affect our main conclusion that there were major differences between the amplitudes of the faster 2AP decay components for the free and complexed DNAs. Anisotropies of the free DNAs exhibited significant picosecond

Table 3. Parameters of Femtosecond Time-Resolved Anisotropy Decays

	DNA hairpin	significant component decay times[a] (anisotropy magnitudes, r)		fundamental anisotropy[c] ($r_o = \sum r$)
free DNA hairpin	HPAP-9	183 (0.18)	~ns (0.13)[b]	0.31
	HPAP-9′	145 (0.13)	~ns (0.13)	0.26
	HPAP-11	172 (0.16)	~ns (0.11)	0.27
	HPAP-loop	130 (0.14)	~ns (0.13)	0.28
	HPAP-48mer	172 (0.14)	~ns (0.22)	0.36
g5p−DNA complex	HPAP-9	92 (0.02)	~ns (0.34)	0.36
	HPAP-9′	82 (0.03)	~ns (0.28)	0.31
	HPAP-11	105−161 (0.025 ± 0.004)	~ns (0.25 ± 0.03)	0.27 ± 0.03
	HPAP-loop	54−107 (0.06 ± 0.02)	~ns (0.29 ± 0.02)	0.35 ± 0.01
	HPAP-48mer	58 (0.03)	~ns (0.17)	0.20

[a]Decay curves were fit with two exponential terms. The shorter decay time is given in picoseconds. The longer decay time was arbitrarily chosen to be at 10 ns because of the limited experimental time window, but its value has little effect on the amplitudes of the two decay times. Ranges of decay times are shown for duplicate measurements of the HPAP-loop complex and for triplicate measurements of the HPAP-11 complex. Anisotropy magnitudes are averages with errors that are the range of duplicate measurements and the standard deviation of triplicate measurements. Anisotropy magnitudes are rounded to the nearest hundredth. [b]Amplitude of a component in the >4 ns time regime. [c]The fundamental anisotropy, which is close to 0.4 for 2AP,[43] varies between ~0.2 and ~0.4 because of experimental uncertainties in the individual anisotropy values.

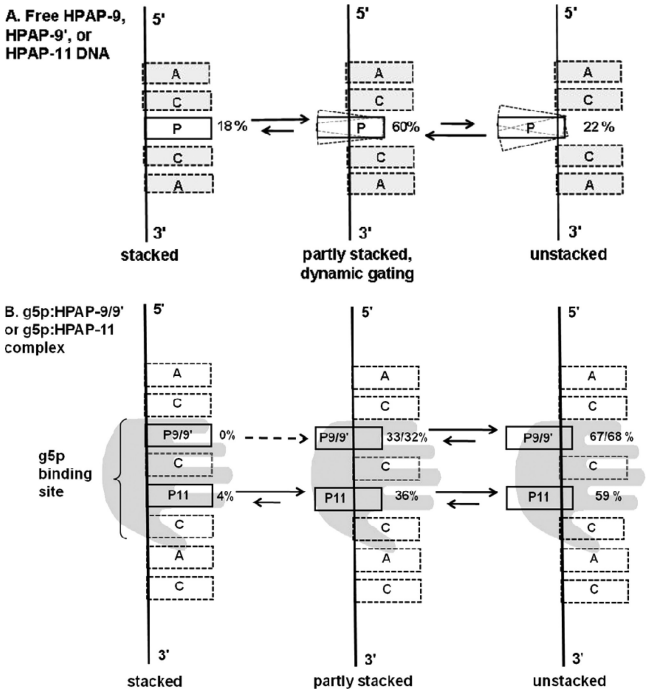

Figure 8. Schematics to illustrate differences in the heterogeneity of populated states occupied by 2AP in two subsite locations of the g5p binding site when bound to 44-nucleotide oligomers. (A) Oligomers HPAP-9, HPAP-9′, and HPAP-11 in the absence of protein each had three similar decay components. (B) Oligomers HPAP-9 and HPAP-9′ when bound by g5p could not be distinguished from each other and had only two decay components, whereas HPAP-11 reproducibly exhibited a third faster decay component with a small amplitude. Similar states for 2AP in the 9th (or 33rd) and 11th positions, in HPAP-9 (or HPAP-9′) and HPAP-11, respectively, are shown together in a given oligonucleotide chain, but this is not meant to imply synchronous movements of the bases in the different positions. Also, the partly stacked conformations are not necessarily intermediates between the stacked and unstacked conformations. The percentages of populations are derived from the amplitudes of decay times in Table 2.

decay components, amounting to approximately one-half of the total anisotropies, due to local motions of the 2AP labels (see Figure 7 and Table 3). There were very small picosecond components to the anisotropy decays of the complexes. Therefore, the states of the 2AP labels that are in equilibrium within the subsites of the g5p binding site were of relatively inflexible conformations and did not appear to involve the more flexible states that existed within the free DNAs. We interpret the unstacked conformation of the 2AP in the complexes (i.e., the 11.3 ns time-resolved decay components of Table 2) as being more restricted than the conformations corresponding to the unstacked, slowest decaying component of the free DNAs. In addition, the faster fluorescent decay components that remain for the bound 2AP in HPAP-9, HPAP-9′, HPAP-11, and HPAP-48mer are consistent with residual base−base stacking, but other mechanisms causing fast static quenching cannot be excluded.

From the equilibrium populations having the two longest fluorescence decay times in Table 2, the $\Delta\Delta G°(22\ °C)$ for converting a 2AP in either subsite location (9/9′ vs 11) from the (presumably stacked) conformation with the faster decay to the unstacked conformation with the slower decay can be calculated. The $\Delta\Delta G°(22\ °C)$ is −0.2 to −0.4 kcal/mol in favor of the unstacked conformation for 2AP labels bound in the two g5p subsites (HPAP-11 and HPAP-9/9′, respectively), compared with an average of 0.7 kcal/mol not in favor of the unstacked conformation in the case of these three free DNAs. In general, the 2AP conformations that exist are not separated by large energy barriers in either the bound or free states. A predominance of unstacked conformations of the 2AP in two subsite locations of the g5p-bound state of the DNA and the existence of unstacked conformations at lower abundance in the free forms of the DNAs suggest that binding of g5p to a lattice site may involve a conformational capture mechanism, analogous to the capture of RNA riboswitch and aptamer conformations by their ligands.[14,15,55] For example, when the bases in a DNA lattice site are arrayed in a suitably unstacked fashion, recognition by g5p might be initially favorable, with access to alternate conformations being available to the bases after binding. The fact that nucleotides in ssDNA can exist in a distribution of conformational states, as shown by the values in Table 2, might also allow g5p to capture different combinations of conformations to satisfy the functional requirement of binding nonspecifically to all ssDNA sequences. However, additional experiments will be needed to assess the importance

dx.doi.org/10.1021/bi2006543 | Biochemistry 2011, 50, 8989−9001

of conformational capture as a general mechanism for binding to ssDNA by g5p and possibly other SSBs.

■ ASSOCIATED CONTENT

Supporting Information

Ultrafast fluorescence decay profiles expanded to show the time up to 10 ps (Figure S1), amplitudes of the faster decay components when anisotropy decay profiles are fit with various slower decay component times (Figure S2), melting profiles of six oligomers (Figure S3), EMSA titrations of six oligomers (Figure S4), comparison of steady-state fluorescence titrations of HPAP-48mer and HPAP-9 (Figure S5), fluorescence emission spectra of HPAP-loop DNA with and without added g5p (Figure S6), ultrafast fluorescence and anisotropy decay profiles for the free HPAP-48mer oligomer and g5p–HPAP-48mer complex (Figure S7), and a discussion of the percentage of DNA saturated in complexes used for femtosecond decay and anisotropy measurements. This material is available free of charge via the Internet at http://pubs.acs.org.

■ AUTHOR INFORMATION

Corresponding Author

*D.M.G.: e-mail, dongray@utdallas.edu; phone, (972) 883-2513; fax, (972) 883-2409. T.X.: e-mail, tianbing.xia@utdallas.edu; phone, (972) 883-6328; fax, (972) 883-2409.

Funding

Support was provided by grants from the Robert A. Welch Foundation (AT-503 to D.M.G. and AT-1645 to T.X.) and by a grant from the THECB Norman Hackerman Advanced Research Program (009741-0015-2007 to T.X.).

Notes

This work was performed by H.-N.N. in partial fulfillment of the requirements for a Ph.D. in the Department of Molecular and Cell Biology, The University of Texas at Dallas.

■ ABBREVIATIONS

2AP, 2-aminopurine; CD, circular dichroism; EMSA, electrophoretic mobility shift assay; EDTA, ethylenediaminetetraacetic acid; BBO, β-barium borate; Ff, F-pilus-specific filamentous bacteriophages (f1, fd, and M13) of *E. coli*; g5p, gene 5 protein; HP, hairpin; HPLC, high-pressure liquid chromatography; %H, percent hyperchromicity; ITC, isothermal titration calorimetry; $K\omega$, intrinsic binding constant K times a cooperativity factor ω for a gene 5 protein dimer; L, free g5p dimer concentration; n, number of nucleotides bound per g5p monomer; N_D, number of gene 5 protein dimers; N_D/S, [g5p dimers]/[DNA strand] molar ratio; Nmer, oligomer with N nucleotides; OB-fold, oligonucleotide/oligosaccharide binding fold; OPA, optical parametric amplifier; RPA, replication protein A; SD, standard deviation; SDS, sodium dodecyl sulfate; SSBs, single-stranded DNA-binding proteins; ssDNA, single-stranded DNA; TAE buffer, 40 mM Tris-acetate (pH 8.4) and 1 mM EDTA; TN buffer, 5 mM Tris-HCl (pH 7.2) and 40 mM NaCl; T_m, melting temperature; Tris-HCl, tris(hydroxymethyl)-aminomethane hydrochloride; UV, ultraviolet.

■ REFERENCES

(1) Daujotytė, D., Liutkevičiūte, Z., Tamulaitis, G., and Klimašauskas, S. (2008) Chemical mapping of cytosines enzymatically flipped out of the DNA helix. *Nucleic Acids Res. 36*, e57.

(2) Wold, M. S. (1997) Replication protein A: A heterotrimeric, single-stranded DNA-binding protein required for eukaryotic DNA metabolism. *Annu. Rev. Biochem. 66*, 61–92.

(3) Wang, X., and Haber, J. E. (2004) Roles of *Saccharomyces* single-stranded DNA-binding protein RPA in the strand invasion step of double-strand break repair. *PLoS Biol. 2*, 104–112.

(4) Mou, T.-C., Gray, C. W., and Gray, D. M. (1999) The binding affinity of Ff Gene 5 protein depends on the nearest-neighbor composition of the ssDNA substrate. *Biophys. J. 76*, 1537–1551.

(5) Gray, D. M. (2000) CD of protein-nucleic acid interactions. In *Circular Dichroism: Principles and Applications* (Berova, N., Nakanishi, K., and Woody, R. W., Eds.) 2nd ed., pp 769–796, John Wiley & Sons, New York.

(6) Gray, D. M., Gray, C. W., Mou, T.-C., and Wen, J.-D. (2002) CD of single-stranded, double-stranded, and G-quartet nucleic acids in complexes with a single-stranded DNA-binding protein. *Enantiomers 7*, 49–58.

(7) Mou, T.-C., Shen, M., Abdalla, S., Delamora, D., Bochkareva, E., Bochkarev, A., and Gray, D. M. (2006) Effects of ssDNA sequences on non-sequence-specific protein binding. *Chirality 18*, 370–382.

(8) Roy, R., Kozlov, A. G., Lohman, T. M., and Ha, T. (2009) SSB protein diffusion on a single-stranded DNA stimulates RecA filament formation. *Nature 461*, 1092–1097.

(9) Zhao, L., and Xia, T. (2007) Direct revelation of multiple conformations in RNA by femtosecond dynamics. *J. Am. Chem. Soc. 129*, 4119–4118.

(10) Zhao, L., and Xia, T. (2009) Probing RNA conformational dynamics and heterogeneity using femtosecond time-resolved fluorescence spectroscopy. *Methods 49*, 128–135.

(11) Avilov, S. V., Godet, J., Piémont, E., and Mély, Y. (2009) Site-specific characterization of HIV-1 nucleocapsid protein binding to oligonucleotides with two binding sites. *Biochemistry 48*, 2422–2430.

(12) Kadakkuzha, B. M., Zhao, L., and Xia, T. (2009) Conformational distribution and ultrafast base dynamics of leadzyme. *Biochemistry 48*, 3807–3809.

(13) Chang, C.-W., Guo, L., Kao, Y.-T., Lia, J., Tan, C., Li, T., Saxena, C., Liu, Z., Wang, L., Sancar, A., and Zhong, D. (2010) Ultrafast solvation dynamics at binding and active sites of photolyases. *Proc. Natl. Acad. Sci. U.S.A. 107*, 2914–2919.

(14) Jain, N., Zhao, L., Liu, J. D., and Xia, T. (2010) Heterogeneity and dynamics of the ligand recognition mode in purine-sensing riboswitches. *Biochemistry 49*, 3703–3714.

(15) Lee, S. W., Zhao, L., Pardi, A., and Xia, T. (2010) Ultrafast dynamics show that the theophylline and 3-methylxanthine aptamers employ a conformational capture mechanism for binding their ligands. *Biochemistry 49*, 2943–2951.

(16) Li, J., Liu, Z., Tan, C., Guo, X., Wang, L., Sancar, A., and Zhong, D. (2010) Dynamics and mechanism of repair of ultraviolet induced (6–4) photoproduct by photolyase. *Nature 466*, 887–890.

(17) Bradrick, T. D., and Marino, J. P. (2004) Ligand-induced changes in 2-aminopurine fluorescence as a probe for small molecule binding to HIV-1 TAR RNA. *RNA 10*, 1459–1468.

(18) Zhao, C., and Marino, J. P. (2007) Synthesis of HIV-1 Ψ-site RNA sequences with site specific incorporation of the fluorescent base analog 2-aminopurine. *Tetrahedron 63*, 3575–3584.

(19) Murzin, A. G. (1993) OB(oligonucleotide/oligosaccharide binding)-fold: Common structural and functional solution for non-homologous sequences. *EMBO J. 12*, 861–867.

(20) Skinner, M. M., Zhang, H., Leschnitzer, D. H., Guan, Y., Bellamy, H., Sweet, R. A., Gray, C. W., Konings, R. N. H., Wang, A. H.-J., and Terwilliger, T. C. (1994) Structure of the gene V protein of bacteriophage f1 determined by multiwavelength X-ray diffraction on the selenomethionyl protein. *Proc. Natl. Acad. Sci. U.S.A. 91*, 2071–2075.

(21) Bochkarev, A., and Bochkarev, E. (2004) From RPA to BRACA2: Lessons from single-stranded DNA binding by the OB-fold. *Curr. Opin. Struct. Biol. 14*, 36–42.

(22) Gray, C. W. (1989) Three-dimensional structure of complexes of single-stranded DNA-binding proteins with DNA. IKe and fd gene 5

proteins form left-handed helices with single-stranded DNA. *J. Mol. Biol. 208*, 57−64.
(23) Russel, M. (1991) Filamentous phage assembly. *Mol. Microbiol. 5*, 1607−1613.
(24) Kansy, J. W., Clack, B. A., and Gray, D. M. (1986) The binding of fd gene 5 protein to polydeoxynucleotides: Evidence from CD measurements for two binding modes. *J. Biomol. Struct. Dyn. 3*, 1079−1110.
(25) Ferrari, M. E., and Lohman, T. M. (1994) Apparent heat capacity change accompanying a nonspecific protein-DNA interaction. *Escherichia coli* SSB tetramer binding to oligodeoxyadenylates. *Biochemistry 33*, 12896−12910.
(26) Sang, B.-C., and Gray, D. M. (1989) Specificity of the binding of fd gene 5 protein to polydeoxyribonucleotides. *J. Biomol. Struct. Dyn. 7*, 693−706.
(27) Terwilliger, T. C. (1996) Gene V protein dimerization and cooperativity of binding to poly(dA). *Biochemistry 35*, 16652−16664.
(28) Hirao, I., Nishimural, Y., Tagawa, Y., Watanabe, K., and Miura, K. (1992) Extraordinarily stable mini-hairpins: Electrophoretical and thermal properties of the various sequence variants of d(GCGAAGC) and their effect on DNA sequencing. *Nucleic Acids Res. 20*, 3891−3896.
(29) Varani, G. (1995) Exceptionally Stable Nucleic Acid Hairpins. *Annu. Rev. Biophys. Biomol. Struct. 24*, 379−404.
(30) Thompson, T. M., Mark, B. L., Gray, C. W., Terwilliger, T. C., Sreerama, N., Woody, R. W., and Gray, D. M. (1998) Circular dichroism and electron microscopy of a core Y61F mutant of the F1 gene 5 single-stranded DNA-binding protein and theoretical analysis of CD spectra of four Tyr → Phe substitutions. *Biochemistry 37*, 7463−7477.
(31) Wong, C., Sridhara, S., Bardwell, J. C., and Jakob, U. (2000) Heating greatly speeds Coomassie blue staining and destaining. *BioTechniques 28*, 426−428, 430, 432.
(32) Day, L. A. (1973) Circular dichroism and ultraviolet absorption of a deoxyribonucleic acid binding protein of filamentous bacteriophage. *Biochemistry 12*, 5329−5339.
(33) Gray, D. M., Hung, S.-H., and Johnson, K. H. (1995) Absorption and circular dichroism spectroscopy of nucleic acid duplexes and triplexes. *Methods Enzymol. 246*, 19−34.
(34) Cavaluzzi, M. J., and Borer, P. N. (2004) Revised UV extinction coefficients for nucleoside-5′-monophosphates and unpaired DNA and RNA. *Nucleic Acids Res. 32*, e13.
(35) Savitzky, A., and Golay, M. J. E. (1964) Smoothing and differentiation of data by simplified least squares procedures. *Anal. Chem. 36*, 1627−1639.
(36) Bailey, W. F., and Monahan, A. S. (1978) Statistical effects and the evaluation of entropy differences in equilibrium processes. *J. Chem. Educ. 55*, 489−493.
(37) Liu, J. D., Zhao, L., and Xia, T. (2008) The dynamic structural basis of differential enhancement of conformational stability by 5′- and 3′-dangling ends in RNA. *Biochemistry 47*, 5962−5975.
(38) Wan, C., Fiebig, T., Schiemann, O., Barton, J. K., and Zewail, A. H. (2000) Femtosecond direct observation of charge transfer between bases in DNA. *Proc. Natl. Acad. Sci. U.S.A. 97*, 14052−14055.
(39) Fiebig, T., Wan, C., and Zewail, A. H. (2002) Femtosecond charge transfer dynamics of a modified DNA base: 2-Aminopurine in complexes with nucleotides. *ChemPhysChem 3*, 781−788.
(40) Pal, S. K., Peon, J., and Zewail, A. H. (2002) Ultrafast decay and hydration dynamics of DNA bases and mimics. *Chem. Phys. Lett. 363*, 57−63.
(41) Pal, S. K., Zhao, L., Xia, T., and Zewail, A. H. (2003) Site- and sequence-selective ultrafast hydration of DNA. *Proc. Natl. Acad. Sci. U.S.A. 100*, 13746−13751.
(42) Andreatta, D., Lustres, J. L. P., Kovalenko, S. A., Ernsting, N. P., Murphy, C. J., Coleman, R. S., and Berg, M. A. (2005) Power-law solvation dynamics in DNA over six decades in time. *J. Am. Chem. Soc. 127*, 7270−7271.
(43) Holmén, A., Nordén, B., and Albinsson, B. (1997) Electronic transition moments of 2-aminopurine. *J. Am. Chem. Soc. 119*, 3114−3121.
(44) Lakowicz, J. R. (2006) *Principles of Fluorescence Spectroscopy*, 3rd ed., p 354, Springer Science, New York.
(45) Kozlov, A. G., and Lohman, T. M. (1998) Calorimetric studies of *E. coli* SSB protein-single stranded DNA interactions. Effects of monovalent salts on binding enthalpy. *J. Mol. Biol. 278*, 999−1014.
(46) Kozlov, A. G., and Lohman, T. M. (1999) Adenine base unstacking dominates the observed enthalpy and heat capacity changes for the *Escherichia coli* SSB tetramer binding to single-stranded oligoadenylates. *Biochemistry 38*, 7388−7397.
(47) Kumaran, S., Kozlov, A. G., and Lohman, T. M. (2006) *Saccharomyces cerevisiae* replication protein A binds to single-stranded DNA in multiple salt-dependent modes. *Biochemistry 45*, 11958−11973.
(48) Manoj, P., Min, C.-K., Aravindakumar, C. T., and Joo, T. (2008) Ultrafast charge transfer dynamics in 2-aminopurine modified double helical DNA. *Chem. Phys. 352*, 333−338.
(49) O'Neill, M. A., Becker, H.-C., Wan, C., Barton, J. K., and Zewail, A. H. (2003) Ultrafast dynamics in DNA-mediated electron transfer: Base gating and the role of temperature. *Angew. Chem. Int. Ed. 42*, 5896−5900.
(50) Bulsink, H., Wijnaendts Van Resandt, R. W., Harmsen, B. J. M., and Hilbers, C. W. (1986) Different DNA-binding modes and cooperativities for bacteriophage M13 gene-5 protein revealed by means of fluorescence depolarisation studies. *Eur. J. Biochem. 157*, 329−334.
(51) King, G. C., and Coleman, J. E. (1988) The Ff gene 5 protein-$d(pA)_{40-60}$ complex: ^{1}H NMR supports a localized base-binding model. *Biochemistry 27*, 6947−6953.
(52) Folkers, P. J. M., van Duynhoven, J. P. M., van Lieshout, H. T. M., Harmsen, B. J. M., van Boom, J. H., Tesser, G. I., Konings, R. N. H., and Hilbers, C. W. (1993) Exploring the DNA binding domain of gene V protein encoded by bacteriophage M13 with the aid of spin-labeled oligonucleotides in combination with ^{1}H-NMR. *Biochemistry 32*, 9407−9416.
(53) Prompers, J. J., Folmer, R. H. A., Nilges, M., Folkers, P. J. M., Konings, R. N. H., and Hilbers, C. W. (1995) Refined solution structure of the Tyr41→His mutant of the M13 gene V protein: A comparison with the crystal structure. *Eur. J. Biochem. 232*, 506−514.
(54) Unruh, J. R., Gokulrangan, G., Lushington, G. H., Johnson, C. K., and Wils, G. S. (2005) Orientational dynamics and dye-DNA interactions in a dye-labeled DNA aptamer. *Biophys. J. 88*, 3455−3465.
(55) Leulliot, N., and Varani, G. (2001) Current topics in RNA−protein recognition: Control of specificity and biological function through induced fit and conformational capture. *Biochemistry 40*, 7947−7956.